International Journal of
Environmental Research and Public Health

MDPI

Article

Spatiotemporal Big Data for $PM_{2.5}$ Exposure and Health Risk Assessment during COVID-19

Hongbin He [1,2], Yonglin Shen [1,3,*], Changmin Jiang [1], Tianqi Li [1], Mingqiang Guo [1,*] and Ling Yao [3]

1 School of Geography and Information Engineering, China University of Geosciences, Wuhan 430074, China; 20161004430@cug.edu.cn (H.H.); 20141000446@cug.edu.cn (C.J.); ltq@cug.edu.cn (T.L.)
2 Institute of International Rivers and Eco-security, Yunnan University, Kunming 650500, China
3 State Key Laboratory of Resources and Environmental Information System, Institute of Geographic Sciences and Natural Resources Research, Chinese Academy of Sciences, Beijing 100101, China; yaoling@lreis.ac.cn
* Correspondence: shenyl@cug.edu.cn (Y.S.); guomingqiang@cug.edu.cn (M.G.)

Received: 31 August 2020; Accepted: 19 October 2020; Published: 21 October 2020

Abstract: The coronavirus disease 2019 (COVID-19) first identified at the end of 2019, significantly impacts the regional environment and human health. This study assesses $PM_{2.5}$ exposure and health risk during COVID-19, and its driving factors have been analyzed using spatiotemporal big data, including Tencent location-based services (LBS) data, place of interest (POI), and $PM_{2.5}$ site monitoring data. Specifically, the empirical orthogonal function (EOF) is utilized to analyze the spatiotemporal variation of $PM_{2.5}$ concentration firstly. Then, population exposure and health risks of $PM_{2.5}$ during the COVID-19 epidemic have been assessed based on LBS data. To further understand the driving factors of $PM_{2.5}$ pollution, the relationship between $PM_{2.5}$ concentration and POI data has been quantitatively analyzed using geographically weighted regression (GWR). The results show the time series coefficients of monthly $PM_{2.5}$ concentrations distributed with a U-shape, i.e., with a decrease followed by an increase from January to December. In terms of spatial distribution, the $PM_{2.5}$ concentration shows a noteworthy decline over the Central and North China. The LBS-based population density distribution indicates that the health risk of $PM_{2.5}$ in the west is significantly lower than that in the Middle East. Urban gross domestic product (GDP) and urban green area are negatively correlated with $PM_{2.5}$; while, road area, urban taxis, urban buses, and urban factories are positive. Among them, the number of urban factories contributes the most to $PM_{2.5}$ pollution. In terms of reducing the health risks and $PM_{2.5}$ pollution, several pointed suggestions to improve the status has been proposed.

Keywords: spatiotemporal big data; empirical orthogonal function (EOF); geographic weighted regression (GWR); population distribution; COVID-19

1. Introduction

Coronavirus disease 2019 (COVID-19) is a lung disease caused by a novel coronavirus first detected in late 2019, which has a significant impact on the regional environment [1–3] and human health [4,5]. Many scholars discussed the clinical manifestations [6] of COVID-19 and the risk factors of death and its detailed clinical course [7,8], providing an important basis for the rapid and accurate diagnosis of COVID-19 patients. Airborne pollutants with diameters less than or equal to 2.5 microns are known as $PM_{2.5}$ or fine particles. Due to the characteristics of small diameter, large-area coverage, strong activity, easy bonding with toxic substances, $PM_{2.5}$ can be suspended in the atmosphere for a long time, severely impacting on the regional environment and Earth's biological cycle [9]. Furthermore, they are prone to provide carriers for toxic substances, e.g., absorbing harmful gases such as polycyclic

aromatic hydrocarbons (PAHs) from industrial exhaust gas and polluted microorganisms, which then enter the human body through breathing, causing harm to the immune system, respiratory tract, cardiovascular and cerebrovascular system, and nervous center system of the human body and causing a series of diseases. With the prevalence of the internet of things (IoT), artificial intelligence (AI) and cloud computing, the spatiotemporal big data, e.g., location-based service (LBS) and place of interest (POI) data, that derived from navigation and positioning, location and trajectory, online car-hailing order, social media network, and macro national economic, are increasing rapidly. The rational and effective use of spatiotemporal big data will play a positive role in understanding influence factors of $PM_{2.5}$ concentration, and quantitatively assessing the population exposure and health risks of $PM_{2.5}$ during COVID-19.

Compared the state-of-the-art studies on $PM_{2.5}$ exposure and health risks, most studies used census-based population data, which ignores the spatial heterogeneity of population, and indirectly leads to lower accuracy. With the rise of the IoT, more and more portable mobile devices are adding LBS, a service that records real-time data about people's activities in space and time. Compared to traditional demographics-based or global positioning system (GPS)-based location recording data, integrated LBS and $PM_{2.5}$ data can improve the assessment of the population exposure and health risks because it can be modeled with high precision by establishing a relationship between $PM_{2.5}$ concentrations and population density. The spatial and temporal distributions of $PM_{2.5}$ have been extensively studied using geostatistical methods [10,11], as well as the pattern of spatial distribution of $PM_{2.5}$ was analyzed. For China, most studies focused on the Jing-Jin-Ji urban agglomeration [12,13], the Yangtze River economic zones [14–16], and the Pearl River Delta region [17], Cheng-Yu urban agglomeration [18]. Studies at the national scale are also increasingly being undertaken. Li et al. [19] used statistical methods and geographic information system (GIS) technology to systematically analyze the $PM_{2.5}$ concentration to discover the spatial and temporal distribution patterns of air pollution in the 161 cities of mainland China in 2014. In addition, Zhang et al. [20] found that $PM_{2.5}$ is associated with an increase in disease morbidity and mortality by examining indicators of the biological effects of $PM_{2.5}$. Fu et al. [21] established an empirical model of human health risk factors caused by excessive $PM_{2.5}$ concentration, and studied the impact of the combination of population spatial distribution and $PM_{2.5}$ spatial distribution on population health. Song et al. [22] used spatiotemporal big data (micro-blog location data) to study the Jing-Jin-Ji urban agglomeration of $PM_{2.5}$ for dynamic exposure and health risk assessment. However, current studies rarely consider the mobility of the population when assessing the $PM_{2.5}$ exposure and health risk, especially in the COVID-19 epidemic.

In this study, a comprehensive assessment of the population exposure, health risks, and driving factors of $PM_{2.5}$ nationwide during the COVID-19 epidemic has been conducted by using high-precision spatiotemporal data. To be specific, the empirical orthogonal function (EOF) is used to analyze the patterns of $PM_{2.5}$ concentrations in China in both the temporal and spatial dimensions. Then, high-precision LBS data are used to explore the potential relationship between Chinese population and $PM_{2.5}$ exposure during the COVID-19 epidemic, and to quantitatively assess the corresponding health risk. In order to quantify the driving factors of $PM_{2.5}$ that impact health risk, this study uses geographically weighted regression (GWR) method to quantify the relationship between POI and $PM_{2.5}$. This study expects to provide comprehensive reference and decision making for better protecting the ecological environment.

2. Materials and Methods

2.1. Study Area and Datasets

As a developing country, China is facing the twofold challenges of economic development and environmental protection. China's economy is sustained growing, with a gross domestic product (GDP) of 990,865 million yuan in 2019, an increase of 67.1% compared with that of 2013. Meanwhile, energy consumption reached 4.86 billion tons of standard coal in 2019, a significant increase over total energy consumption in 2013. Environmental protection is a basic national policy and an important strategy

for achieving sustainable development, and is an integral part of comprehensive pollution control and environmental protection planning. According to the China Air Quality Improvement Report. (2013–2018) [23] published by the Ministry of Ecology in 2019, overall air quality in China improved from 2013 to 2018, and the emissions of major air pollutants decreased significantly. The average concentration of $PM_{2.5}$ in 74 cities using ambient air quality standards fell by 42%. China has also actively formulated a national climate change strategy to promote environmental improvement by reducing carbon emissions.

The data involved in this study mainly include $PM_{2.5}$ monitoring station data, POI data, national secondary industry output value data, a digital elevation model (DEM), LBS data, and urban population data (Figure 1).

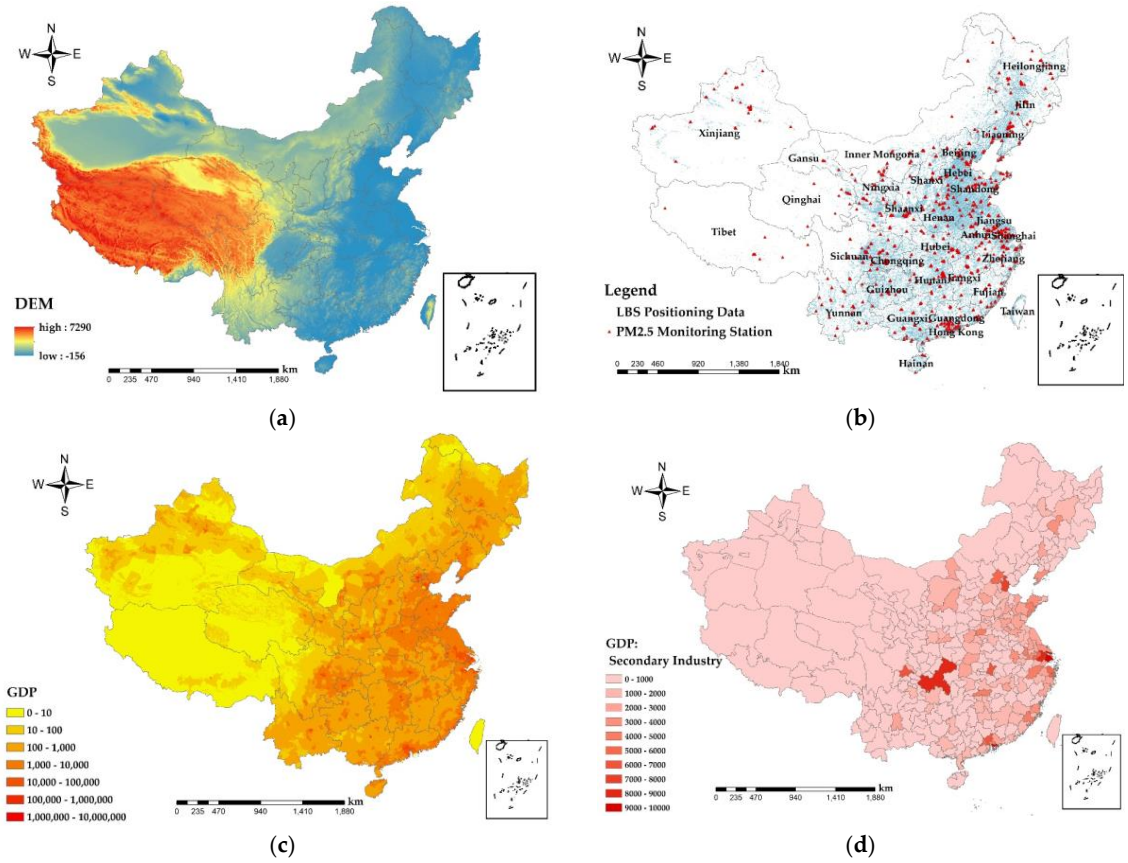

Figure 1. Study area and data, (**a**) elevation, (**b**) spatial distribution of particulate matter ($PM_{2.5}$) monitoring sites and Tencent's location-based services (LBS) in China, (**c**) gross domestic product (GDP), and (**d**) secondary production.

(1) $PM_{2.5}$ concentration was obtained from the National Real-time Urban Air Quality Release System of the China environmental monitoring general station [24] (national air quality monitoring stations were in only 190 cities in 2014, and since then all cities have been covered). Data from 1670 stations were acquired until 2020. To present the spatiotemporal distribution of $PM_{2.5}$, a GIS-based spatial interpolation is applied to convert to 1×1 km grid.

(2) POI data, were derived from the National Bureau of Statistics [25] and the local bureau of statistics, mainly including six factors that affect the distribution of $PM_{2.5}$ concentration, including urban GDP, green space, road area, the number of urban taxis, the number of urban buses, and the number of urban factories. Urban GDP includes primary, secondary, and tertiary industry GDP, in units of 10,000 yuan. The urban green area contains public, residential, unit affiliated, protective, production, road green, and scenic forest areas, and the unit is hectares.

The road area includes urban main roads, secondary, and branch roads, with a unit of 10,000 m^2. The number of urban taxis and buses is the total number of vehicles in operation at the end of each year. The number of urban factories contains capital-intensive industrial, labor-intensive, resource-intensive, and knowledge-technology-intensive factories. The time period of all POI data was from 2014 to 2017.

(3) LBS data came from Tencent location big data [26], which use positioning technology to obtain a position in the whole scene. Relying on the full coverage and high accuracy of LBS data, to study the impact of the COVID-19 epidemic on population mobility, this study selected four main time nodes because of the limited permission to access the Tencent's services, i.e., 25 December 2020, 11 January 2020, 7 March 2020, and 3 April 2020. On 25 December 2019 people in China were producing and living normally. The turning point of the COVID-19 outbreak was 11 January 2020. Since this period, the number of patients infected with COVID-19 has continued to increase. It is also the time node when the Spring Festival travel season began. The peak number of COVID-19 infections was on 7 March 2020. On 3 April 2020 the COVID-19 epidemic in China was basically under control, and the life of the people returned to normal. The temporal resolution of LBS data is the hour, and the data accumulatively obtained 297,535,280 positioning times of 4,194,304 positioning points. The study uses the grid mapping method of the geographic information system to map the positioning data to a 1×1 km grid, and the number of positioning of all the positioning points in the same grid is summed to obtain the population of the grid.

(4) Auxiliary data contained 2017 national secondary industry output value data and 2019 national urban population data from the National Bureau of Statistics [25], and DEM data were from the Resource and Environment Science and Data Center [27].

2.2. Empirical Orthogonal Function (EOF)

EOF was first proposed by the statistician Pearson in 1902 [28], and is known as the spatiotemporal decomposition in geological applications [29–35]. The absolute value of the time series coefficient represents the degree of air pollution, the closer it comes to zero, better the air quality is. This study firstly calculated the average $PM_{2.5}$ concentration $\overline{P_{ij}}$ of 1657 stations in 367 prefecture-level cities in 31 provinces of China (excluding Hong Kong, Macao, and Taiwan) from 2014 to 2019, then estimates the $PM_{2.5}$ concentrations anomalies P_{mn} and the covariance matrix A_{jk},

$$P_{mn} = \left(P_{ij} - \overline{P_{ij}}\right) \tag{1}$$

$$A_{mk} = \frac{1}{m} \cdot P_{mn} \cdot (P_{nk})^T \tag{2}$$

where i, m represents the year, $i = m = 1, 2, \ldots, 6$; and j, k, n is the station at each city, $j = k = n = 1, 2, \ldots, 1657$; A_{mk} is a real symmetric, positive definite square matrix of order n. The Jacobi method was used to solve the eigenvalues $\lambda_1 \geq \lambda_2 \geq \lambda_3 \geq \cdots \geq \lambda_k \geq \cdots \geq \lambda_n$ and eigenvectors of the covariance matrix A_{jk}. The eigenvalues and corresponding eigenvectors can be formulated by,

$$A_{nn} \cdot X_k = \lambda_k \cdot X_k \tag{3}$$

where X_{nn} is the natural orthogonal function of the original field P_{mn}, and its time series coefficient can be expressed as,

$$T_{mn} = P_{mn} \cdot X_{nn} = \begin{bmatrix} T_{11} & T_{12} & \ldots & T_{1n} \\ T_{21} & T_{22} & \ldots & T_{2n} \\ \ldots & \ldots & \ldots & \ldots \\ T_{m1} & T_{m2} & \ldots & T_{mn} \end{bmatrix} \tag{4}$$

where T_{mn} and P_{mn} are matrices with the same order. The original field can be represented as a linear combination of natural orthogonal functions,

$$P_{mn}(t,s) = T_{mn}(t) \cdot X_{nn}(s) \quad (5)$$

where s represents the space point and t represents the observation time. In general, the most important information in the original field can be fully reflected by the first few eigenvectors and time series coefficients.

2.3. Particulate Matter ($PM_{2.5}$) Exposure Assessment

LBS data are adopted to conduct $PM_{2.5}$ exposure assessment and health risk analysis, since LBS data are with a daily temporal resolution, which can accurately reflect the population mobility [36]. In this study, the LBS data are employed as an indicator to quantify the spatial and temporal patterns of population distribution. Due to the differences of socio-economic development and mobile internet penetration among different cities, the population dynamic distribution of each city is estimated separately. Since the daily total location data contains duplicate data, in order to eliminate the impact of duplicate data, this study redistributes the total population data of each city based on the hourly LBS data location data (Equation (6)), and generates the density map of LBS data by aggregating all the geotagged records of each grid.

$$Pop_{pq} = \frac{P_{pq}}{\sum_{p=1}^{z} P_{pq}} \cdot Tol_p \quad (6)$$

where p_{pq} is the positioning quantity of Tencent's position data in the p grid; z is the total number of pixels in the city; Tol_p is the total population of the city. For each city, the $PM_{2.5}$ exposures were assessed via a pixel-based method (Equation (7)) [37], which can effectively reduce the potential zoning effect of the modifiable areal unit problem (MAUP) [38].

$$E_{PM} = \frac{Pop_p \times PM_p}{\sum_{p=1}^{n} Pop_p} \quad (7)$$

where PM_p stands for $PM_{2.5}$ concentration; Pop_p is the data redistributed based on LBS data. E_{PM} represents a population-weighted assessment of $PM_{2.5}$ exposure.

2.4. Health Risk Assessment of $PM_{2.5}$ during COVID-19 Outbreaks

In this study, the health risk of $PM_{2.5}$ was evaluated using the long-term risk assessment value recommended by the World Health Organization (WHO). With reference to the assessment method of the WHO, the health risk of residents was assessed using the $PM_{2.5}$ concentration obtained and the current status of population distribution.

$$E = \beta \cdot (c - c_0) \cdot E_0 \cdot P_p \quad (8)$$

where E represents the potential risk of disease of residents under the current $PM_{2.5}$ concentration; β is the proportion of the mortality caused by the change of $PM_{2.5}$. In this study, the mortality rate of $PM_{2.5}$ decreased by 10 μg/m^3 by 6% [39]; c is the actual $PM_{2.5}$ concentration; c_0 is the referenced $PM_{2.5}$ concentration; E_0 is the health effect of residents under the referenced concentration. The mortality rate in the population census (7.14%) was selected in this study; and P_p is the population at the current location.

2.5. Geographic Weighted Regression (GWR)

General linear and non-linear regression were widely used in previous studies to analyze the relation between two groups of variables, However, taking consideration of heterogeneity of POI data,

an advanced method of GWR is adopted in this study to eliminate spatial heterogeneity and improve the fitting results. Fotheringham et al. [40], based on the thinking behind the local smooth GWR model, is put forward [41–43]. The GWR model can be formulated by,

$$y_p = \beta_0\left(u_p,\ v_p\right) + \beta_1\left(u_p,\ v_p\right)\cdot x_{p1} + \cdots + \beta_q\left(u_p,\ v_p\right)\cdot x_{pq} + \varepsilon_s \quad (9)$$

where $\left(u_p,\ v_p\right)$ represents the spatial position p, $(p = 1, 2, \ldots, 367)$. The spatial regression coefficient of $\beta_0, \beta_1, \ldots, \beta_q$ is a function of position space coordinates which indicates the degree that spatial independent variables affected dependent variables. ε_s is a deviation, it represents the degree of deviation of two variables. y_p is $PM_{2.5}$ concentration. x_{pq} is POI data.

3. Results and Discussion

This study focuses on the following four parts: (1) through spatial autocorrelation analysis and EOF decomposition, discussing the temporal and spatial characteristics of $PM_{2.5}$ concentration; (2) based on the spatiotemporal distribution of $PM_{2.5}$, calculating the population exposure of $PM_{2.5}$ based on Tencent LBS data during the COVID-19 epidemic; (3) adopting the long-term health assessment method of air quality recommended by the World Health Organization (WHO) to assess the health risk of $PM_{2.5}$ during the COVID-19 epidemic; (4) the relationship between $PM_{2.5}$ and its driving factors were quantitatively analyzed using the GWR method to address the health threat posed by $PM_{2.5}$ to human beings, and relevant measures are proposed to address these driving factors.

3.1. EOF Analysis of Monthly $PM_{2.5}$ Concentration

This study used the EOF spatiotemporal decomposition of $PM_{2.5}$ station observations from 367 cities during 2014–2019 to reveal the spatial and temporal patterns of $PM_{2.5}$. Because the first feature vector has a cumulative contribution of variance greater than 70% (Figure 2), it was chosen to characterize the spatial pattern of $PM_{2.5}$ concentration.

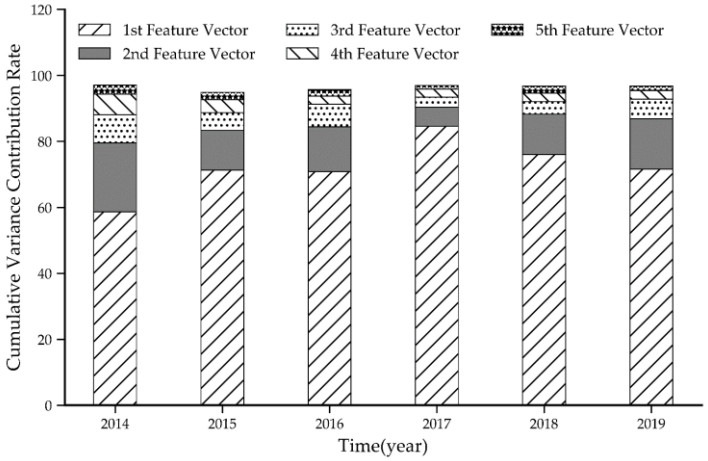

Figure 2. Variance contribution rate of each feature vector.

The time series coefficient reflects the variations of $PM_{2.5}$ concentration over time. Figure 3 shows the change in time series coefficients corresponding to the $PM_{2.5}$ eigenvector for each month during the six-year period of 2014–2019. The time series coefficients of $PM_{2.5}$ concentration have the same changing trend, and the difference between months is significant, with the peak intervals located in the month of January from 2015–2019. The valley value of the time series coefficient of $PM_{2.5}$ concentration is located in August 2014, August 2015, August 2016, August 2017, September 2018 and August 2019. Overall, the time series coefficients for each year show a U-shaped distribution characteristic of increase after an initial decrease. In China, precipitation is scarce in January, February and December each

year, and the phenomenon of "temperature inversion" is prominent, which seriously hinders the horizontal transportation and vertical diffusion of air, and easily causes pollutants to gather in the surface layer, making $PM_{2.5}$ pollution more serious [44]. Meanwhile, the temperature in January, February, and December is low, and people use more electricity to keep warm. Insufficient combustion of fossil fuels by facilities such as thermal power plants and coal furnaces causes a substantial increase in $PM_{2.5}$ concentrations [45]. In addition, the large amount of straw burning also contributes to a high concentration of $PM_{2.5}$ [46]. According the variation of time series coefficient from 2014–2019, values of 2018 and 2019 are relatively low, indicating that $PM_{2.5}$ concentration declined significantly from 2018.

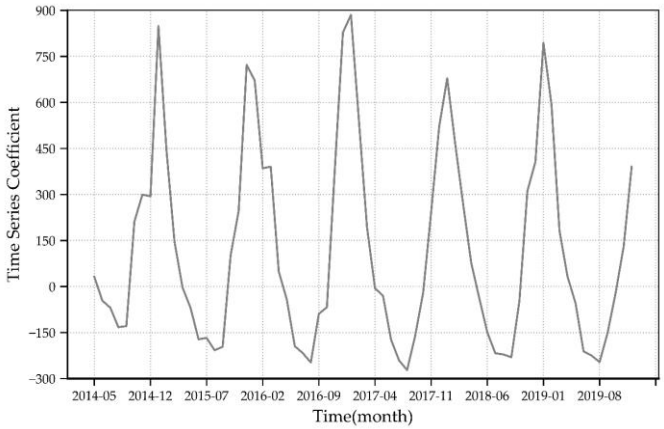

Figure 3. Monthly feature vector time series coefficients during 2014–2019.

The spatial distribution of the EOF first feature vector reflects the overall spatial distribution characteristics of $PM_{2.5}$ concentrations on the monthly scale. From Figure 4, it can be seen that the high $PM_{2.5}$ concentration areas in China in 2014 were mainly concentrated in the Jing-Jin-Ji urban agglomeration and Heilongjiang Province, and the high $PM_{2.5}$ concentration areas from 2015 to 2019 were concentrated in Hebei Province, Henan Province, and Hubei Province and the spatial distribution of $PM_{2.5}$ concentration sprawling from the area to its surroundings. As seen in Figure 1a, the Jing-Jin-Ji urban agglomeration, Henan, and Shandong Province are located in the lower elevation plain, and surrounded by mountains, which are not conducive to the atmospheric transmission of $PM_{2.5}$. In addition, the irrational industrial structure within these regions leads to the emission of endogenous pollutants [47]. Since 2015, the Xinjiang Autonomous Region (XAR) started to appear as the region of second highest $PM_{2.5}$ concentration, with peaks in Urumqi and Kashgar in 2019. On the one hand, because XAR is far from the ocean, precipitation is scarce, and it has China's largest desert, the Taklamakan Desert, whose wind fields basically dominate in the low precipitation and drought of XAR [48]. On the other hand, the population of XAR is growing rapidly, and at a rate higher than the national average [49]. Increasing winter heating facilities and population growth has had a serious impact on the fragile environment of the XAR, which causes serious $PM_{2.5}$ pollution. In addition, there are many mines around Urumqi. With the development of Midong District, high-pollution industries such as petrochemicals, chlor-alkali chemicals, coal, electricity and coal chemicals have gathered here [50], and large freight vehicles have a large traffic flow, which is affected by secondary particles and coal. The impact of smoke and vehicle emissions is greater, resulting in serious $PM_{2.5}$ pollution around Urumqi. $PM_{2.5}$ concentrations reached troughs in southwest Yunnan Province, southwest Sichuan Province, Tibet Autonomous Region, and southeast coastal areas. On the one hand, the underdeveloped economy (Figure 1c) and low industrial output (Figure 1d) in these regions are the predominant reasons. On the other hand, the terrain of these areas is rugged (Figure 1a), and the primary industry, tertiary industry service industry and tourism are mainly developed, which have less impact on $PM_{2.5}$, so the level of $PM_{2.5}$ pollution in these areas is low.

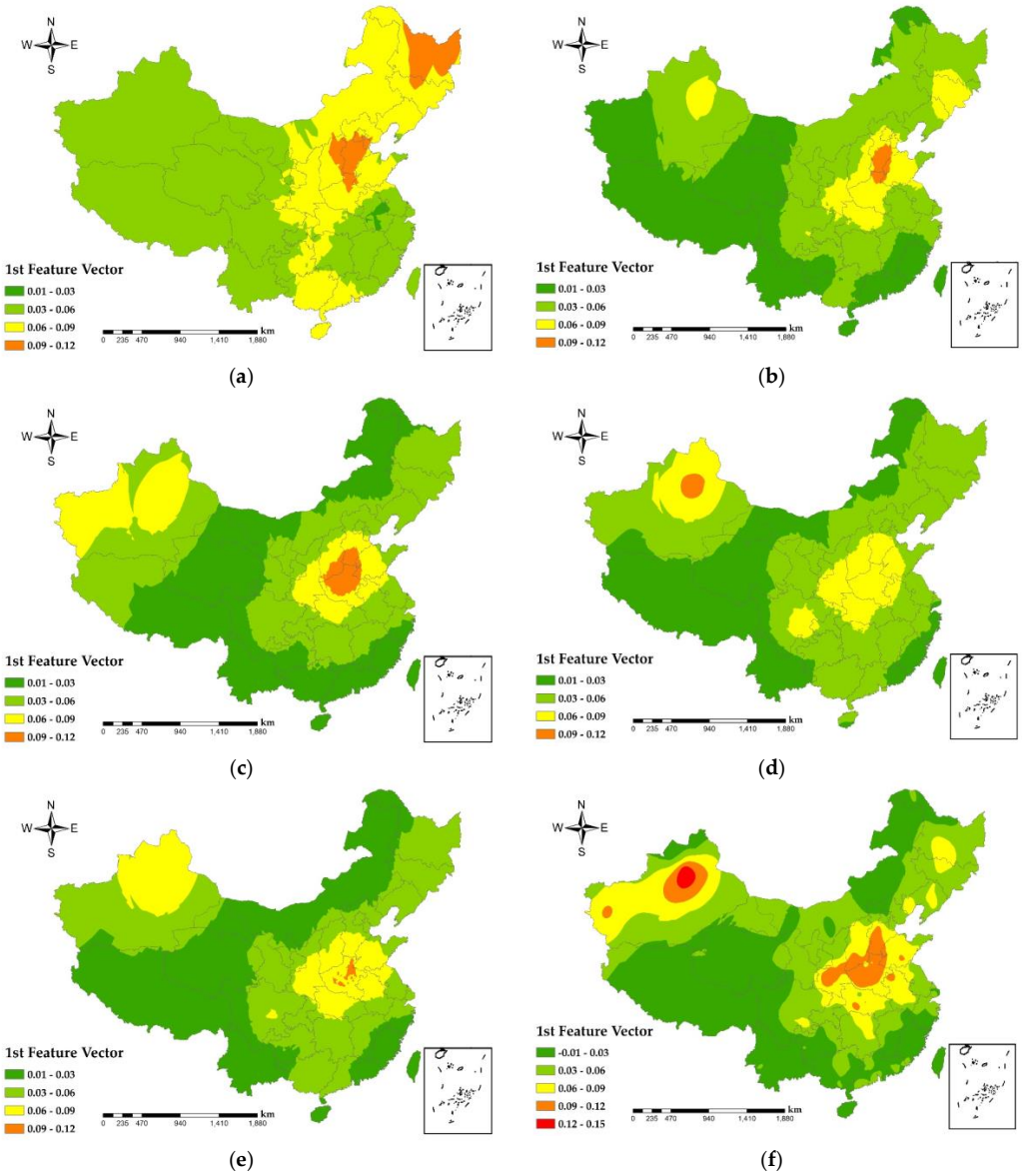

Figure 4. Spatial distribution of the first feature vector of monthly $PM_{2.5}$ concentration during 2014–2019. (**a**) 2014; (**b**) 2015; (**c**) 2016; (**d**) 2017; (**e**) 2018; and (**f**) 2019.

3.2. $PM_{2.5}$ Population Exposure Assessment

In order to analyze the changes in $PM_{2.5}$ population exposure during the COVID-9 epidemic. Based on the spatiotemporal distribution of $PM_{2.5}$, this research selects LBS big data during the COVID-19 epidemic, and uses a GIS-based method to allocate the acquired population data to a grid of 1 × 1 km. On this basis, we have calculated a population density distribution map (Figure 5).

As shown in Figure 5, the maximum value areas of national population density in December 2019 are distributed in the North China Plain, the Yangtze River Delta urban agglomeration, the Pearl River Delta urban agglomeration, the Chengdu-Chongqing urban agglomeration and Central China. The minimum areas are mainly distributed in the western and northwestern regions of China. In January 2020, the maximum value areas are concentrated in the North China Plain, the Yangtze River Delta urban agglomeration, the Pearl River Delta urban agglomeration, the Chengdu-Chongqing urban agglomeration, and Central China. January 2020 compared to December 2019, when the range of maximum value areas is decreasing, and population density shows a trend of spreading from high value areas to the low. Statistics by the State Railway Administration [51] and the Civil Aviation

Administration of China (CAAC) [52] show that the number of transported passengers was 321,862,000 in January 2020. The degree of population mobility is large, and the trend of mobility is the movement of people from first-tier and new first-tier cities such as Beijing, Shanghai, Guangzhou, Shenzhen, and Wuhan to surrounding smaller cities.

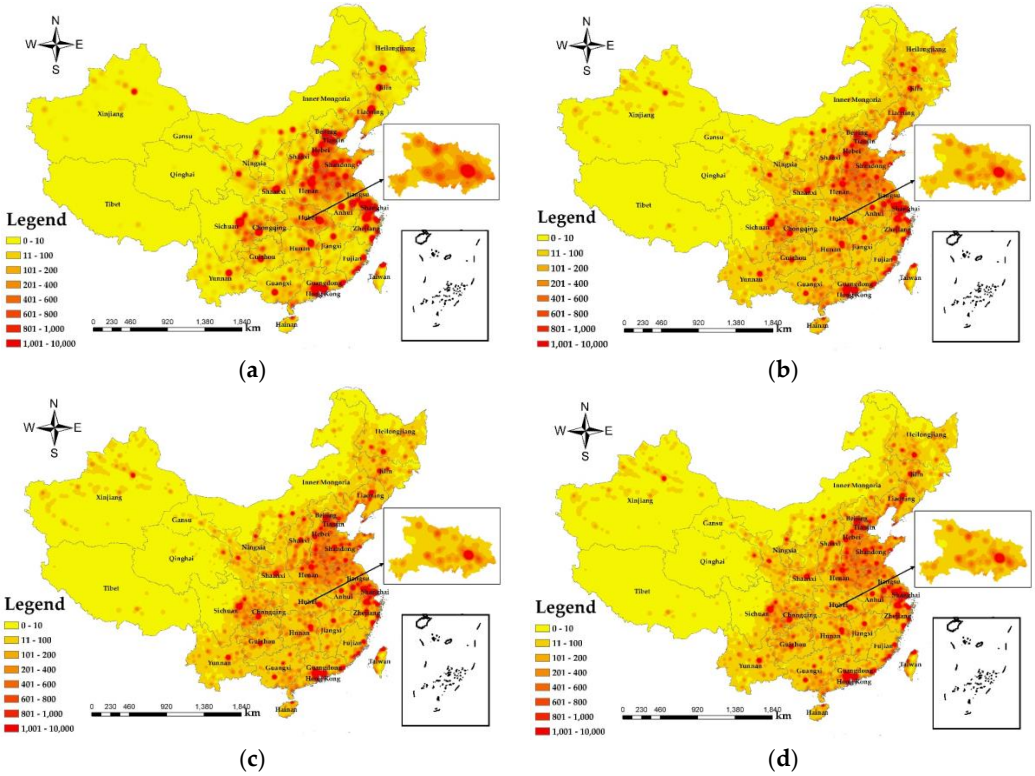

Figure 5. Population density distribution map based on LBS data. (**a**) 25 December 2019; (**b**) 11 January 2020; (**c**) 7 March 2020; and (**d**) 3 April 2020.

In March 2020, the scope of the region of maximum population density compared to January 2020. The region of greatest values is concentrated in the Yangtze River Delta, Pearl River Delta, and Chengdu-Chongqing urban agglomeration. As a result of the COVID-19 epidemic, the number of COVID-19 infected patients in the country peaked in March 2020, while there were no large number of new suspected infections, access to various community units in the country was strictly controlled, and road, railway and air transport authorities also took corresponding measures to restrict population movement. Enterprises in some cities gradually resumed work and production in March, but employees had to be quarantined for 14 days for observation before resuming work and production, resulting in lower urban population density in first-tier and new first-tier cities in China. In April 2020, the maximum population density areas of large cities were concentrated in the Jing-Jin-Ji urban agglomerations, the Yangtze River Delta, the Pearl River Delta, the Chengdu-Chongqing urban agglomeration, Wuhan and Changsha, with an increasing trend compared to March 2020, but there is still a gap compared to the population density in January 2020, and with the state's push for enterprises to resume work and production, most of the enterprises have started production activities in April 2020, and the population density range has an increasing trend in the first-tier and new first-tier cities. In general, the more densely populated areas are mainly distributed in the middle and lower reaches of the Yangtze River Delta (Shanghai, Jiangsu, Zhejiang, Anhui, etc.), the Pearl River Delta (Guangzhou, Shenzhen, Hong Kong Special Administrative Region of China, Macao Special Administrative Region of China, etc.), the Jing-Jin-Ji urban agglomeration (Beijing, Tianjin, Hebei, etc.), and the Chengdu-Chongqing urban agglomeration (Chongqing, Chengdu, Mianyang, etc.). The total economic output and per capita GDP are relatively high in the region. The population distribution

throughout China is characterized by a relatively high concentration of people in the eastern part of the country and a relatively sparse population in the western part.

At the end of 2019, a sudden outbreak of COVID-19 epidemic, bringing a heavy blow. From the comparison between Figure 5a,b, the population density of Hubei changed greatly from 25 December 2019 to 11 January 2020, and the change in Wuhan City was particularly noticeable. The official report by the Wuhan Municipal Railway Bureau on 11 January 2020, the stations under the jurisdiction of the Wuhan Railway Bureau sent 570,000 passengers, including about 100,000 student passengers. As can be seen from Figure 6c, the population density of Hubei has also declined significantly compared to January 2020, with the range of population density in Wuhan shrinking considerably. Due to the COVID-19 outbreak in Wuhan, the city of Wuhan has been blocked to management since 24 January 2020, and the degree of population movement has decreased, reducing the spatial range of the maximum value of population density in Wuhan. From Figure 5d, the spatial extent of population density in cities of Hubei, except Wuhan, tends to expand, accompanied by a gradual intensification of population mobility with the resumption of work in Hubei.

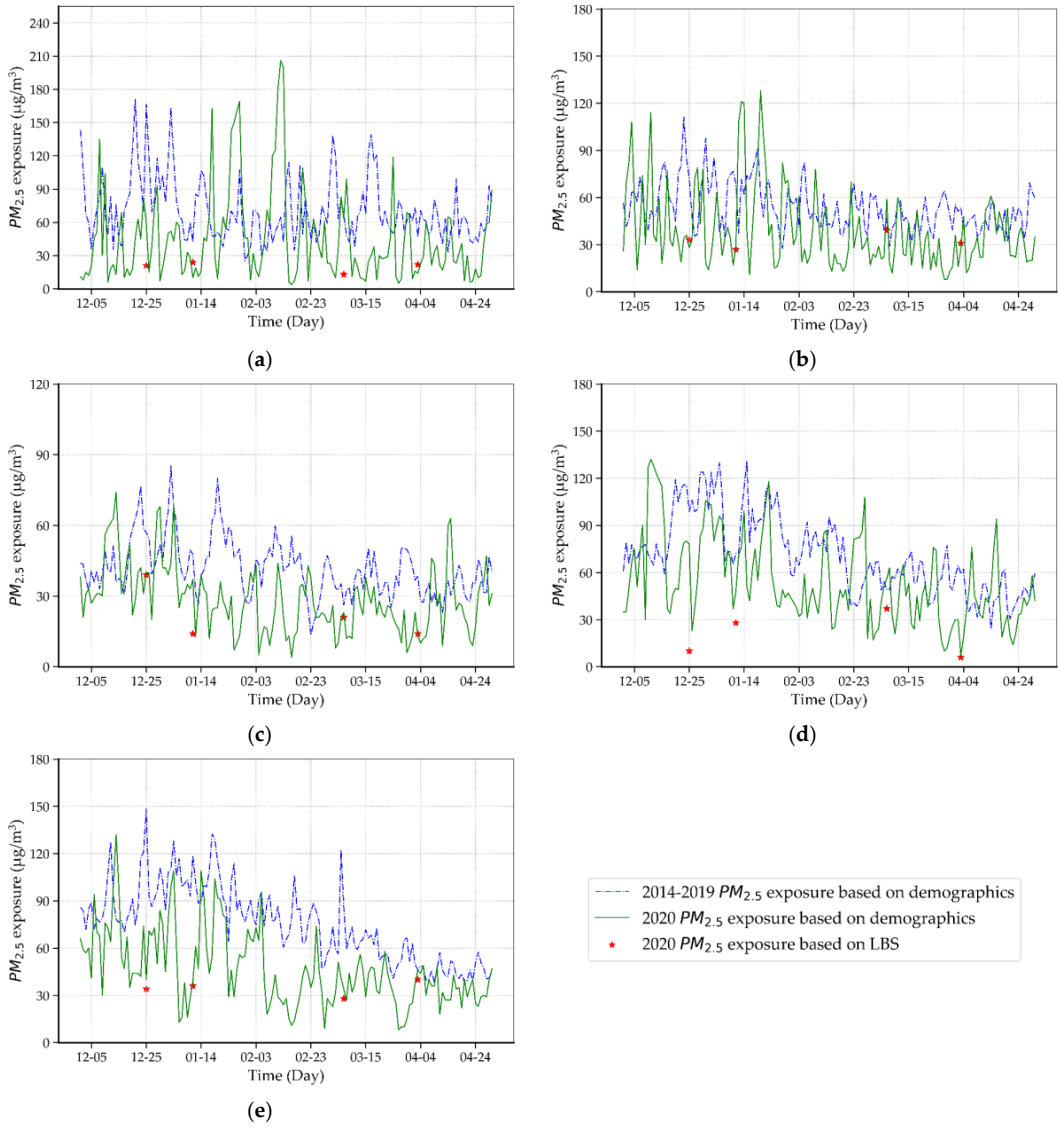

Figure 6. $PM_{2.5}$ exposure in typical population-intensive cities based on demographic and LBS data. (**a**) Beijing, (**b**) Shanghai, (**c**) Guangzhou, (**d**) Chengdu, and (**e**) Wuhan.

To further quantify the changes of the COVID-19 situation on $PM_{2.5}$ exposure and the effectiveness of LBS data, data analysis on five typical population-intensive cities of China (i.e., Beijing, Shanghai, Guangzhou, Chengdu, and Wuhan) was performed, in which the daily $PM_{2.5}$ ground monitoring station data [24], demographic data and LBS data were used. In Figure 6, green curves are daily $PM_{2.5}$ exposure based on demographic data for the period of December 2019 to April 2020 (the duration of COVID-19); by contrast, blue curves are the reference of $PM_{2.5}$ exposure using historical average data (December 2014 to April 2019); marks (red star) represent LBS-based $PM_{2.5}$ exposure on four dates mentioned above.

The influence of the COVID-19 situation on air pollution can be concluded by the comparison of demographic-based $PM_{2.5}$ exposure, i.e., the result in the duration of COVID-19 (green curve) and the result in the historical average (blue curve). Take Wuhan for example, as show in Figure 6e, we found that the $PM_{2.5}$ exposure in Wuhan during the COVID-19 pandemic saw a significantly drop due to the community containment measures. Similarly, cities such as Beijing, Shanghai, Guangzhou, Chengdu, follow the same pattern. The effectiveness of LBS data can be concluded by the comparison of demographic-based $PM_{2.5}$ exposure in the duration of COVID-19 (green curve) and LBS-based $PM_{2.5}$ exposure on four dates (red star). Although we only obtained LBS data at four key time nodes because of access restrictions, the trend of LBS-based $PM_{2.5}$ exposure (red star) is consistent with demographic-based $PM_{2.5}$ exposure (green curve) in these cities. It demonstrates that LBS data on four key dates can characterize the variation of $PM_{2.5}$ exposure well during the COVID-19 pandemic.

As shown in Figure 7, the areas with the highest exposure values on 25 December 2019 occurred in Henan, Hebei, Beijing, the northwestern part of Shandong, the Pearl River Delta, Chengdu, Chongqing, and the capital cities of the Northeast, the exposure values of other cities are relatively low. The areas with the largest exposure values on 11 January 2020 were mainly concentrated in Henan, Beijing, Tianjin, Hebei, Shanghai, Heilongjiang, and the Pearl River Delta. The area with the highest $PM_{2.5}$ exposure on 7 March 2020 appeared around Shanghai. The maximum value on 3 April 2020 appeared in the Pearl River Delta, Wuhan and surrounding areas of Shanghai. According to the trend of the exposure values of $PM_{2.5}$ from December 2019 to April 2020, it can be seen that the exposure values of large cities such as the Jing-Jin-Ji urban agglomeration, the Pearl River Delta, the Yangtze River Delta, and the Chengdu-Chongqing urban agglomeration have maintained at a relatively high level. From December 2019 to April 2020 in these regions, the exposure of $PM_{2.5}$ gradually decreased. Because these areas were central cities for economic development, with a large population density and dense urban space, $PM_{2.5}$ is difficult to diffuse, the values of exposure are large. From Figure 7a,b, the $PM_{2.5}$ exposure in large cities in January 2020 is lower than that in December 2019. It is related to the Spring Festival travel. With the migration of the population, $PM_{2.5}$ exposure in the Jing-Jin-Ji urban agglomeration relatively reduced. Combined with the spatial distribution of $PM_{2.5}$, the reason for the decrease in the exposure of $PM_{2.5}$ in March 2020 compared with January 2020 is related to the control measures issued by government in response to the COVID-19 epidemic. When the COVID-19 occurred, all provinces across the country (autonomous regions and municipalities directly under the central government) launched a first-level emergency response to major public health emergencies. All communities, streets, villages, and towns across the country have implemented community isolation through grid management, and the flow of people has been greatly reduced. In addition, the provinces announced that in addition to guaranteeing the operation of public utilities (e.g., water supply, gas supply, power supply, communication and other industries), epidemic prevention and control (e.g., medical equipment, medicines, protective products production and sales), the people's daily life (e.g., supermarket stores, food production and supply and other industries) and other enterprises other than those related to important national economy and people's livelihood are all shut down. $PM_{2.5}$ exposure was enhanced in April 2020 compared to March 2020, particularly in Hunan, Hubei, Jiangxi, Yunnan and the Pearl River Delta, due to the fact that with the vast majority of the country's enterprises' after more than a month of adjustment, most companies have regained their original capacity, accompanied by the

population movement caused by the resumption of production and the enhanced plant emissions led to an uptick in $PM_{2.5}$ exposure in April 2020.

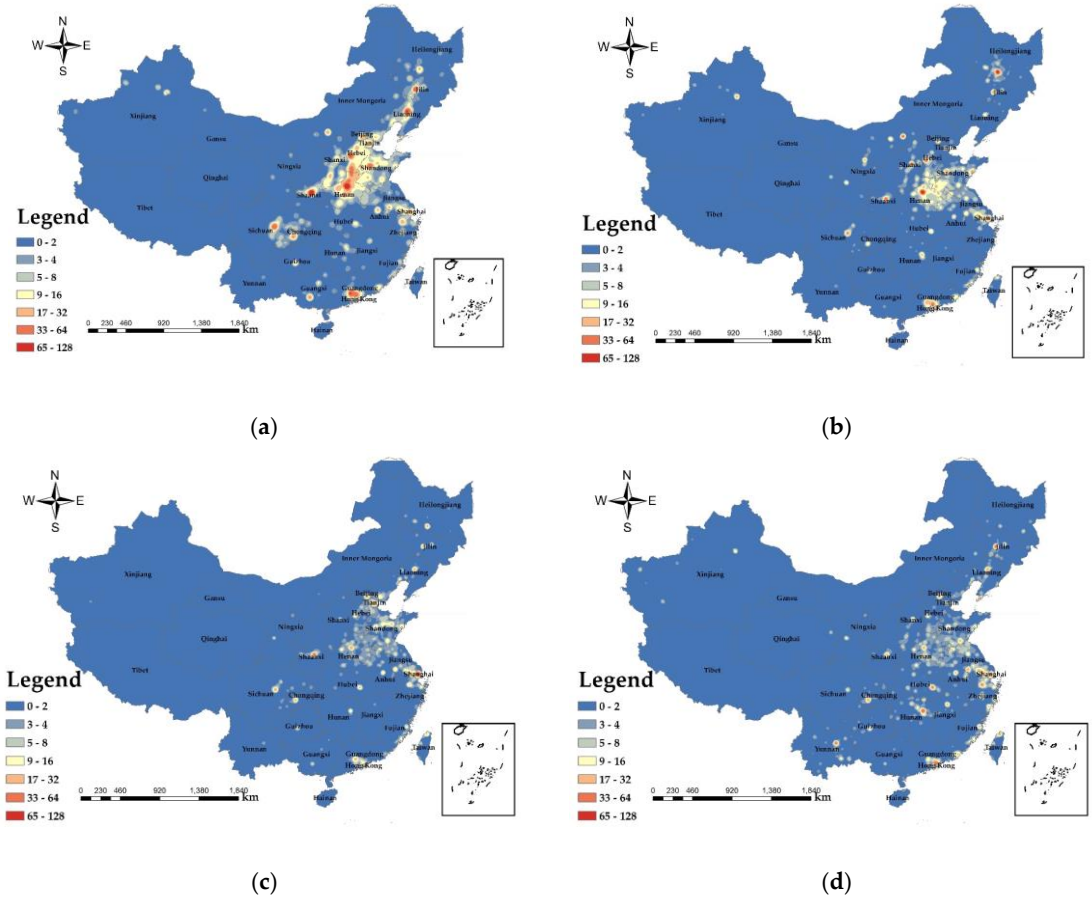

Figure 7. $PM_{2.5}$ exposure assessment value (**a**) 25 December 2019; (**b**) 11 January 2020; (**c**) 7 March 2020; and (**d**) 3 April 2020.

3.3. Health Risk Assessment of $PM_{2.5}$ during COVID-19 Outbreaks

The results are based on the health risk assessment of $PM_{2.5}$, and the potential risks of disease from $PM_{2.5}$ shown in the study results all exclude diseases due to the COVID-19 epidemic. The results of $PM_{2.5}$ health risks in China (Figure 8) show that the maximum potential death toll in December 2019 was 139,424, and the areas with high $PM_{2.5}$ health risks cover the largest area. In March 2020 and April 2020, the impact of $PM_{2.5}$ was lower than that in December 2019 and January 2020. In April 2020, areas with high health risks covered the lowest area, and the maximum potential death toll was 33,462. Compared with the decrease of 105,962 people in December 2019, the decline was relatively large. In terms of geographical distribution, the health risks of $PM_{2.5}$ in the western region are significantly lower than those in the central and eastern regions. The areas with higher $PM_{2.5}$ health risks are mainly concentrated in Beijing, Tianjin, Hebei, Henan, Chengdu, Chongqing, Pearl River Delta, northwestern XAR and Shanghai. According to the population density map based on LBS data (Figure 5), the population during the Spring Festival transport in 2020 will migrate from first-tier cities and new first-tier cities to small cities. According to data from the Beijing Railway Administration, during the Spring Festival travel period, Beijing sent a total of 8,274,100 passengers, and the population density in Beijing decreased. Population migration has reduced the population density of first-tier cities and new first-tier cities, reducing $PM_{2.5}$ exposure and reducing the health risks caused by $PM_{2.5}$. With the evolution of the COVID-19 epidemic, communities across the country were blocked between the end of January 2020 and March 2020, traffic on the roads was reduced, airports, railway stations

and other places of passenger access were strictly controlled, and population movement was reduced, resulting in a reduced health risk from $PM_{2.5}$.

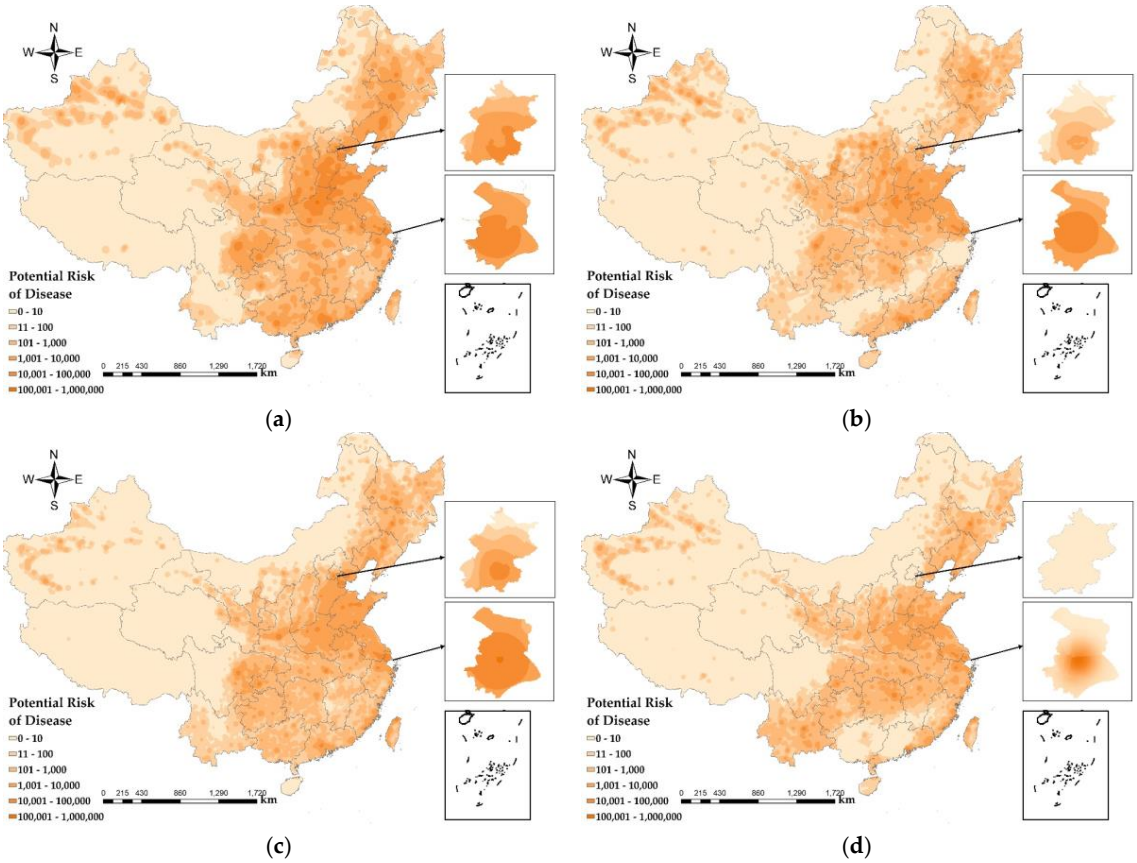

Figure 8. $PM_{2.5}$ health risks assessment. (**a**) 25 December 2019; (**b**) 11 January 2020; (**c**) 7 March 2020; and (**d**) 3 April 2020.

The health risk caused by $PM_{2.5}$ was low in the Tibet Autonomous Region, Qinghai, western Sichuan, northwestern Gansu, and central XAR. The COVID-19 epidemic did not have a significant impact on the health risk of $PM_{2.5}$. From the topography (Figure 1a) and population density map (Figure 5) of the study area, it can be found that these areas have complex topography and a large degree of undulation, which are not suitable for human habitation, making the population density lower and the health risk caused by lower $PM_{2.5}$ concentrations in these areas smaller. In addition, the GDP per capita (Figure 1c) in these regions is low, and the output value of the secondary industry (Figure 1d) is also low, making economic development relatively backward. Moreover, these regions have primary agriculture, animal husbandry, fishery, and tertiary tourism as the pillar industries of their economies, and there is little air pollution caused by $PM_{2.5}$ from large industries, so the health risk caused by $PM_{2.5}$ is relatively low.

3.4. Driving Factors Affecting $PM_{2.5}$ Concentration

$PM_{2.5}$ poses a threat to human health, in order to explore the impact of $PM_{2.5}$ caused by anthropogenic activities and aids the reduction of health risk, the study selected six driving factors (i.e., GDP, road area, green area, number of taxis, number of buses, and number of factories) from POI data and used the GWR method to quantify the impact of these variables on $PM_{2.5}$. In order to effectively explore the primary driving factors on $PM_{2.5}$ concentration, this study respectively selects the adaptive Gaussian Akaike information criterion (AIC) index (determine the best bandwidth

through the minimum information criterion) to be the kernel function and bandwidth of the GWR model, the correlation between the above driving factors and $PM_{2.5}$ concentration was analyzed.

The difference in spatial regression coefficients between $PM_{2.5}$ and various variables reveals the spatial heterogeneity of $PM_{2.5}$ concentration. The spatial regression coefficient of the GWR model reflects the degree of influence of each variable on the $PM_{2.5}$ concentration (Figure 9). When the spatial regression coefficient is positive, it means that the variable is positively correlated with the $PM_{2.5}$ concentration, and the larger the variable is, the greater the impact on $PM_{2.5}$, and vice versa. From the parameter estimation and validation results of the GWR model (Table 1), coefficients of determination (R^2) of the six explanatory variables are above 60%, indicating that the GWR model can better fit the relationship between $PM_{2.5}$ concentration and each variable.

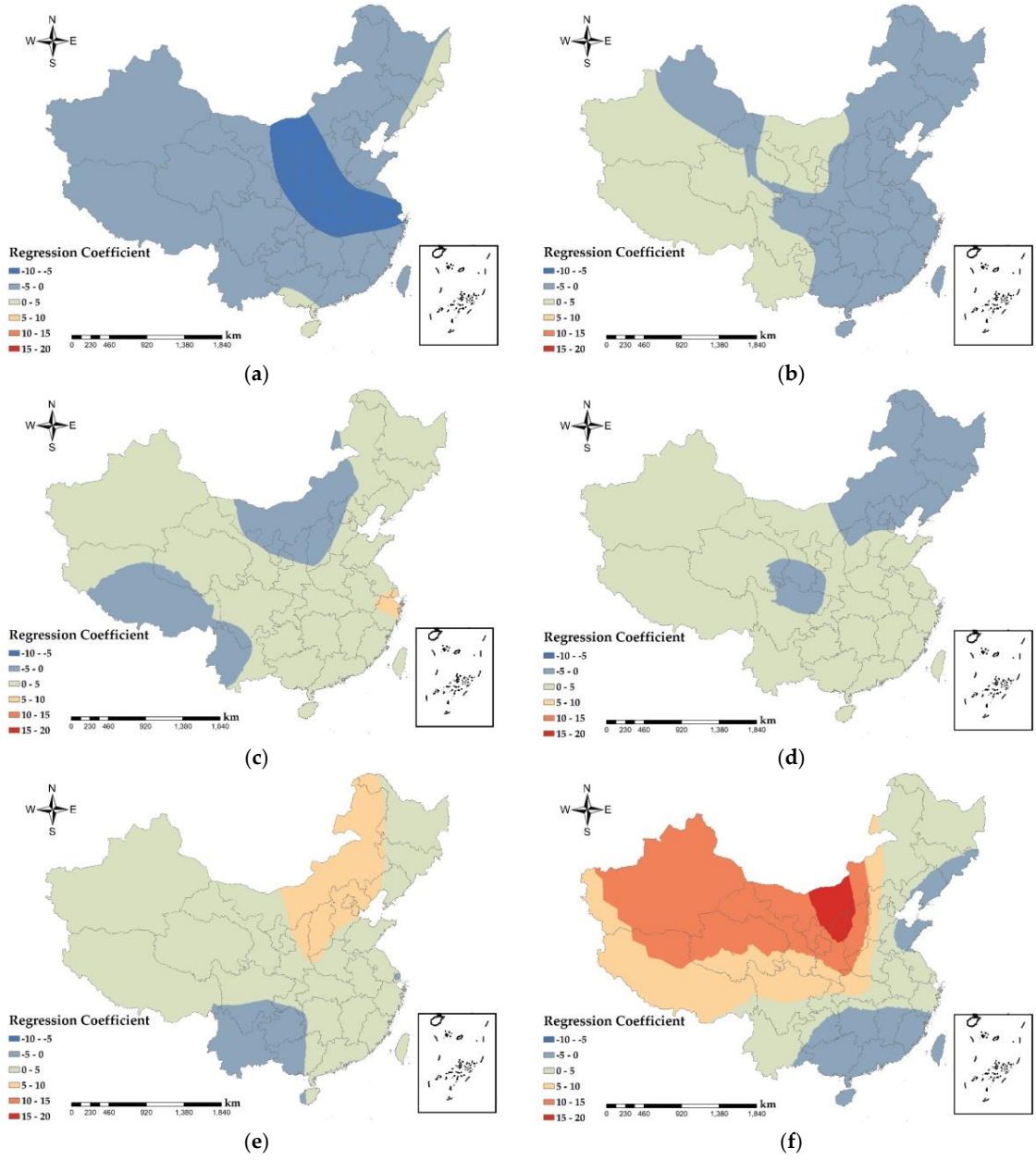

Figure 9. Spatial distribution of regression coefficient ($\times 10^{-3}$) between $PM_{2.5}$ concentration and six explanatory variables. (**a**) urban GDP; (**b**) the area of urban green space; (**c**) road area; (**d**) number of taxis; (**e**) number of buses; and (**f**) number of factories.

Table 1. Estimation and validation of regression results of the geographically weighted regression (GWR) model.

Year	AICc	R^2	Adjusted R^2	Residual Squares
2014	2094.78	0.6759	0.6328	19,078.16
2015	2095.02	0.6910	0.6501	19,473.78
2016	2107.93	0.6303	0.5869	20,026.23
2017	1977.24	0.6738	0.6315	13,311.88

From Figure 9a, the national $PM_{2.5}$ concentration and GDP show a negative correlation (Table 2), indicating that the GDP is high and the corresponding $PM_{2.5}$ concentration is low. The most obvious performance is the urban agglomeration in the middle and lower reaches of the Yangtze River, with the largest absolute value of the regression coefficient. The higher the total urban GDP is, the more attention is paid to the reduction of $PM_{2.5}$ pollution. Regression coefficients ranged from -10 to -5×10^{-3} in areas such as Ningxia Hui Autonomous Region and central Inner Mongolia, where industry is underdeveloped (Figure 1d), the economy is mainly based on primary and tertiary services, and urban $PM_{2.5}$ emissions are low, so GDP and $PM_{2.5}$ show a strong negative correlation. In the southern part of Guangxi Zhuang Autonomous Region and the three provinces of Northeast China, with correlation coefficients between 0 and 5, as the output value of secondary industries in these regions was larger (Figure 1d), and $PM_{2.5}$ emissions from factories were higher, so GDP showed a weak positive correlation with $PM_{2.5}$.

Table 2. Mean value of spatial regression coefficient of GWR model ($\times 10^{-3}$).

Year	Urban GDP	Road Area	Green Space Area	Taxis	Buses	Factories
2014	−6.3	2.1	−0.8	1.7	1.9	7.4
2015	−4.8	1.7	−0.5	1.1	2.3	3.3
2016	−0.5	1.4	−0.4	0.8	2.8	3.1
2017	−1.7	1.1	−0.4	0.4	1.9	0.8

As shown in Figure 9b, urban green areas in South China, East China, Central China, North China, Chengdu-Chongqing urban agglomeration showed negative correlation with $PM_{2.5}$, with correlation coefficients between -5×10^{-3} and 0, indicating that the larger the urban green area, the lower the urban $PM_{2.5}$ concentration. Green plants can not only absorb air pollutants such as dust, sulfide, nitrous oxide, etc., but also the coronal layer of the plant will reduce the speed of wind and block particles in the air. Plant leaves will absorb dust during respiration and photosynthesis. Official data assumes that in an acre of forest planted with 100 trees, 22−60 tons of dust can be absorbed in a year [53]. As a result, urban greenery has a stronger cleaning and air purification function. In the southwest and the west, except for most of the Chengdu-Chongqing urban agglomeration and the northwest, there is a weak positive correlation between the urban green area and $PM_{2.5}$, and the correlation coefficient is between 0 and 5×10^{-3}. Since these areas are located in the first and second terrain (Figure 1a), the climatic conditions and precipitation conditions are not conducive to large-scale vegetation growth. Most vegetation types are grasslands and low shrubs, and the absorption effect of $PM_{2.5}$ is significantly weak, while the absorption intensity of $PM_{2.5}$ by tall vegetation are intensive in the eastern region [54].

As shown in Figure 9c–e, road area and the numbers of urban taxis and buses show a positive correlation with $PM_{2.5}$ concentration (Table 2). The average regression coefficient between road area and $PM_{2.5}$ is between 0 and 5×10^{-3} The population density of Inner Mongolia Autonomous Region, western Yunnan and Tibet Autonomous Region is low due to topography (Figure 1a), climate, and other factors (Figure 5). The roads are scattered, giving the road area and $PM_{2.5}$ a positive correlation. The regression coefficients for the number of urban taxis and $PM_{2.5}$ ranged from -5×10^{-3} to 0, with a weak negative correlation in Northeast China, where industry contributed the most to $PM_{2.5}$ due to the concentrated distribution of heavy industry in the region (Figure 1d). The regression coefficient between the number of urban buses and $PM_{2.5}$ is from 0 to 5×10^{-3} and the Jing-Jin-Ji urban

agglomeration has a strong positive correlation with Shanxi and eastern Inner Mongolia, with the regression coefficient from 5×10^{-3} to 10×10^{-3}. Road area is proportional to urban traffic emissions, with higher emissions ($PM_{2.5}$, nitrogen oxides, carbon oxides, etc.) from urban traffic with major road. According to the China Mobile Source Environmental Management Annual Report (2019) released by the Ministry of Ecology and Environment, China has been the world's largest producer and seller of motor vehicles for 10 consecutive years and, in 2018, the total amount of four pollutants emitted from motor vehicles in the country was initially accounted for 40.653 million tons. This includes 442,000 tons of particulate matter. Automobiles are the main contributors to air pollution emissions from motor vehicles [55]. The topography of Yunnan, Guizhou, and southwestern Sichuan (Figure 1a) resulted in a weak negative correlation between the number of bus and $PM_{2.5}$.

From Figure 9f there is a significant positive correlation between the number of factories in Central, North, Southwest and Northwest China on $PM_{2.5}$, with regression coefficients between 0 and 20×10^{-3}, with the strongest correlation in Shanxi and Central Inner Mongolia. The distribution of secondary industry values in China (Figure 1d) shows that these regions have higher secondary industry emissions. The greater the number of urban factories, the higher the emissions of pollutants (nitrogen oxides, carbon oxides, $PM_{2.5}$, etc.) resulting from the factories' production activities. The spatial regression coefficients of the number of factories and $PM_{2.5}$ show an increasing trend from east to west of China, while the South China show a weak negative correlation trend, indicating that South China pays attention to the emission of $PM_{2.5}$ from factories. Meanwhile, South China is close to the ocean, and the $PM_{2.5}$ concentration generated by factories is positively influenced by the sea breeze that accompanies the ocean currents [56].

The quantitative analysis of the driving factors of $PM_{2.5}$ found that the number of urban factories has the greatest impact on $PM_{2.5}$, indicating that industrial emissions dominated the China's $PM_{2.5}$ pollution. In terms of reducing the health risks and pollution prevention measures caused by $PM_{2.5}$, industrial emissions should be controlled. Launching laws and regulations for $PM_{2.5}$ prevention and control, and formulating relevant standards for industrial waste gas and waste emissions from factories, is necessary. The relevant departments should ensure the implementation of the system. The government promotes the location of new factory sites, increases planning for $PM_{2.5}$ prevention and control in industrial parks, and provides technical support for replacing new clean equipment in factories, while the authorities will increase the supply of clean energy such as electricity and natural gas to reduce reliance on traditional energy sources in factories and reduce $PM_{2.5}$ emissions. Vegetation coverage is an important part of urban ecological construction. Relevant planning departments should make reasonable plans for vegetation planting areas around factories and inside cities to prevent the spread of $PM_{2.5}$ from further harming surrounding residents' health, because trees play a unique ecological function in the purification of atmospheric fine particles.

4. Conclusions

In this paper, we have evaluated the population exposure and health risk of $PM_{2.5}$ in the context of the COVID-19 epidemic, as well as spatiotemporal distribution and driving factors of $PM_{2.5}$ from spatiotemporal big data, including station monitoring of $PM_{2.5}$ concentration, urban POI, and LBS data. The EOF study of the national monthly $PM_{2.5}$ distribution pattern and its evolution in 2014–2019 found that, the time series coefficients of the first feature vector of monthly $PM_{2.5}$ in 2014–2019 showed obvious characteristics, and the time series coefficients showed a downward and then upward trend from year to year, roughly in a U-shaped distribution. In terms of spatial distribution, $PM_{2.5}$ concentrations in central and northern China are relatively higher than those in the surrounding areas, and the distribution pattern shows attenuation from central and northern China to its surrounding areas. From 2014 onwards, $PM_{2.5}$ gradually changed from one center (Central China and North China) to two centers (Central China, North China and XAR). The population density distribution based on the LBS data in China shows that the eastern areas are concentrated and the western areas are relatively sparse. In March and April 2020, most of the $PM_{2.5}$ concentration were below 35 $\mu g/m^3$, which is

caused by the control measures on population movement and industrial production in the cities during the COVID-19 epidemic. The health risk of $PM_{2.5}$ in the western region is significantly lower than that in central and eastern regions. After the outbreak of COVID-19, the domestic health risk caused by $PM_{2.5}$ significantly reduced. The GWR of $PM_{2.5}$ with GDP, urban green space, road area, number of urban taxis, number of urban buses and number of urban factories demonstrates that GDP and urban green space were negatively correlated with $PM_{2.5}$, while road area, number of urban taxis, number of urban buses and number of urban factories were positively correlated with $PM_{2.5}$. In terms of reducing the health risks and pollution prevention measures brought about by $PM_{2.5}$, it is recommended that relevant authorities restrict factory emissions and promote new energy transportation and encourage residents to travel green.

Author Contributions: H.H. was responsible for setting up experiments, completing the experiments and retrieving data and wrote the initial draft of the manuscript; Y.S. principally conceived the idea for the study, and was responsible for the design of the study, writing and editing of this manuscript; C.J., T.L. and L.Y. participated in the experimentation, writing and/or editing of this manuscript; M.G. responsible in some form in the concept, and editing of this manuscript. All authors have read and agreed to the published version of the manuscript.

Funding: This work is partially supported by a grant from State Key Laboratory of Resources and Environmental Information System, and by the National Natural Science Foundation of China under Grant No. 41771380, 41701446, and 41971356.

Acknowledgments: Thanks to the China Environmental Monitoring Station for the $PM_{2.5}$ data released in the national city air quality real-time release system (http://106.37.208.233:20035), and the Tencent-based location service (http://heat.qq.com/) and spatiotemporal big data and POI data provided by the National Bureau of Statistics (http://data.stats.gov.cn/).

Conflicts of Interest: The authors declare no conflict of interest.

References

1. Becker, S.; Soukup, J.M. Exposure to urban air particulates alters the macrophage-mediated inflammatory response to respiratory viral infection. *J. Toxicol. Environ. Health Part. A* **1999**, *57*, 445–457.
2. Yongjian, Z.; Jingu, X.; Fengming, H.; Liqing, C. Association between short-term exposure to air pollution and COVID-19 infection: Evidence from China. *Sci. Total Environ.* **2020**, 138704.
3. Lelieveld, J.; Evans, J.S.; Fnais, M.; Giannadaki, D.; Pozzer, A. The contribution of outdoor air pollution sources to premature mortality on a global scale. *Nature* **2015**, *525*, 367–371. [CrossRef] [PubMed]
4. World Health Organization. *Home Care for Patients with COVID-19 Presenting with Mild Symptoms and Management of Their Contacts: Interim Guidance, 17 March 2020*; World Health Organization: Geneve, Switzerland, 2020.
5. Wu, Z.; McGoogan, J.M. Characteristics of and important lessons from the coronavirus disease 2019 (COVID-19) outbreak in China: Summary of a report of 72 314 cases from the Chinese Center for Disease Control and Prevention. *JAMA* **2020**, *323*, 1239–1242. [CrossRef]
6. Guan, W.; Ni, Z.; Hu, Y.; Liang, W.; Ou, C.; He, J.; Liu, L.; Shan, H.; Lei, C.; Hui, D.S.C.; et al. Clinical characteristics of coronavirus disease 2019 in China. *N. Engl. J. Med.* **2020**, *382*, 1708–1720. [CrossRef]
7. Zhou, F.; Yu, T.; Du, R.; Fan, G.; Liu, Y.; Liu, Z.; Xiang, J.; Wang, Y.; Song, B.; Gu, X.; et al. Clinical course and risk factors for mortality of adult inpatients with COVID-19 in Wuhan, China: A retrospective cohort study. *Lancet* **2020**, *395*, 1054–1062. [CrossRef]
8. Chan, J.F.-W.; Yuan, S.; Kok, K.-H.; To, K.K.-W.; Chu, H.; Yang, J.; Xing, F.; Liu, J.; Yip, C.C.-Y.; Poon, R.W.-S.; et al. A familial cluster of pneumonia associated with the 2019 novel coronavirus indicating person-to-person transmission: A study of a family cluster. *Lancet* **2020**, *395*, 514–523. [CrossRef]
9. He, K.; Yang, F.; Ma, Y.; Zhang, Q.; Yao, X.; Chan, C.K.; Cadle, S.; Chan, T.; Mulawa, P. The characteristics of $PM_{2.5}$ in Beijing, China. *Atmos. Environ.* **2001**, *35*, 4959–4970. [CrossRef]
10. Matějíček, L.; Engst, P.; Jaňour, Z. A GIS-based approach to spatio-temporal analysis of environmental pollution in urban areas: A case study of Prague's environment extended by LIDAR data. *Ecol. Model.* **2006**, *199*, 261–277. [CrossRef]

11. Chuanglin, F.; Zhenbo, W.; Guang, X.U. Spatial-temporal characteristics of $PM_{2.5}$ in China: A city-level perspective analysis. *J. Geogr. Sci.* **2016**, *26*, 1519–1532.
12. Lei, Z.; Jianjun, W.; Ruijing, J.; Liang, N. Investigation of Temporal-Spatial Characteristics and Underlying Risk Factors of $PM_{2.5}$ Pollution in Beijing-Tianjin-Hebei Area. *Res. Environ. Sci.* **2016**, *29*, 483–493.
13. He, X.; Ma, J.; Xu, J. Simulation of a Heavy $PM_{2.5}$ Pollutant Event over Beijing-Tianjin-Hebei Region in October 2014. In *Meteorological Monthly*; Meteorological Office: Beijing, China, 2016.
14. Mian, Y.; Yin, W. Spatial-temporal characteristics of $PM_{2.5}$ and its influencing factors in the Yangtze River Economic Belt. In *China Population, Resources and Environment*; Elsevier: Amsterdam, The Netherlands, 2017.
15. Bai, L.; Jiang, L.; Zhou, H.; Chen, Z. Spatiotemporal Heterogeneity of Air Quality Index and Its Socio-economic Factors in the Yangtze River Economic Belt. *Res. Soil Water Conserv.* **2019**, *26*, 312–319.
16. Bai, L.; Jiang, L.; Chen, Z. Spatio-Temporal Characteristics of $PM_{2.5}$ and Its Influencing Factors of the Urban Agglomeration in the Middle Reaches of the Yangtze River. In *Resources and Environment in the Yangtze Basin*; Science Press: Beijing, China, 2018.
17. Bai, L.; Jiang, L.; Liu, Y. Spatio-Temporal Characteristics of Environmental Pressures of the Urban Agglomeration in the Middle Reaches of the Yangtze River—A Case Study Based on Industrial SO_2 Emissions. *Econ. Geogr.* **2017**, *37*, 174–181.
18. Xiao, K.; Wang, Y.; Wu, G.; Fu, B.; Zhu, Y. Spatiotemporal characteristics of air pollutants (PM_{10}, $PM_{2.5}$, SO_2, NO_2, O_3, and CO) in the inland basin city of Chengdu, southwest China. *Atmosphere* **2018**, *9*, 74. [CrossRef]
19. Li, M.; Ren, X.; Yu, Y.; Zhou, L. Spatiotemporal pattern of ground-level fine particulate matter ($PM_{2.5}$) pollution in mainland China. *China Environ. Sci.* **2016**, *36*, 641–650.
20. Zhang, W.; Cui, J.; Qi, Q. Advances on the biological effect indices for fine particles ($PM_{2.5}$) in air. *J. Hyg. Res.* **2001**, *30*, 379–382.
21. Fu, C.H.; Wang, W.J.; Tang, J. Study on Demographic Spatial Distribution of Health Risks Caused by $PM_{2.5}$: A Case from Shenzhen. *China Soft Sci.* **2014**, *9*, 78–91.
22. Song, Y.; Huang, B.; He, Q.; Chen, B.; Wei, J.; Mahmood, R. Dynamic assessment of PM2. 5 exposure and health risk using remote sensing and geo-spatial big data. *Environ. Pollut.* **2019**, *253*, 288–296. [CrossRef]
23. Ministry of Ecology and Environment of the People's Republic of China. *China Air Quality Improvement Report. (2013–2018)*; China Environmental Monitoring: Beijing, China, 2019; pp. 24–25.
24. China National Environmental Monitoring Centre. Available online: http://106.37.208.233:20035 (accessed on 3 April 2020).
25. National Bureau of Statistics. Available online: https://data.stats.gov.cn/ (accessed on 3 April 2020).
26. Tencent LBS. Available online: http://heat.qq.com/ (accessed on 3 April 2020).
27. Resource and Environment Science and Data Center. Available online: http://www.resdc.cn/ (accessed on 3 April 2020).
28. Pearson, K. On lines and planes of closest fit to systems of points in space. *Philos. Mag.* **1901**, *2*, 559–572. [CrossRef]
29. Chang, J.C.; Mak, M. A Dynamical Empirical Orthogonal Function Analysis of the Intraseasonal Disturbances. *J. Atmos. Sci.* **1993**, *50*, 613–630. [CrossRef]
30. North, G.R. Empirical Orthogonal Functions and Normal Modes. *J. Atmos. Sci.* **1984**, *41*, 879–887. [CrossRef]
31. Kendrick, C.M.; Koonce, P.; George, L.A. Diurnal and seasonal variations of NO, NO2 and $PM_{2.5}$ mass as a function of traffic volumes alongside an urban arterial atmospheric environment. *Atmos. Environ.* **2015**, *122*, 133–141. [CrossRef]
32. Reason, C.J.C.; Allan, R.J.; Lindesay, J.A.; Ansell, T.J. ENSO and Climatic signals across the Indian Ocean basin in the global context. *Int. J. Clim.* **2000**, *20*, 1285–1327. [CrossRef]
33. Xu, H.; Xiao, Z.; Chen, K.; Tang, M.; Zheng, N.; Li, P.; Yang, N.; Yang, W.; Deng, X. Spatial and temporal distribution, chemical characteristics, and sources of ambient particulate matter in the Beijing-Tianjin-Hebei region. *Sci. Total Environ.* **2019**, *658*, 280–293. [CrossRef] [PubMed]
34. Smith, W.L.; Weisz, E.; Kireev, S.V.; Zhou, D.K.; Li, Z.; Borbas, E.E. Dual-Regression Retrieval Algorithm for Real-Time Processing of Satellite Ultraspectral Radiances. *J. Appl. Meteorol. Clim.* **2012**, *51*, 1455–1476. [CrossRef]
35. Peak, J.E.; Wilson, W.E.; Elsberry, R.L.; Chan, J.C.L. Forecasting Tropical Cyclone Motion Using Empirical Orthogonal Function Representations of the Environmental Wind Fields. *Mon. Weather Rev.* **1986**, *114*, 2466–2477. [CrossRef]
36. Xu, W.; He, F.; Li, H.; Zhong, L.J. Spatial and temporal variations of $PM_{2.5}$ in the Pearl River Delta. *Res. Environ.* **2014**, *27*, 951–957.

37. Shen, Y.; Yao, L. PM2. 5, population exposure and economic effects in urban agglomerations of China using ground-based monitoring data. *Int. J. Environ. Res. Public Health* **2017**, *14*, 716. [CrossRef]
38. Ho, H.C.; Wong, M.S.; Yang, L.; Shi, W.; Yang, J.; Bilal, M.; Chan, T.-C. Spatiotemporal influence of temperature, air quality, and urban environment on cause-specific mortality during hazy days. *Environ. Int.* **2018**, *112*, 10–22. [CrossRef]
39. World Health Organization. *WHO Air Quality Guidelines for Particulate Matter, Ozone, Nitrogen Dioxide and Sulfur Dioxide: Global Update 2005: Summary of Risk Assessment*; World Health Organization: Geneva, Switzerland, 2006.
40. Brunsdon, C.; Fotheringham, A.S.; Charlton, M.E. Geographically Weighted Regression: A Method for Exploring Spatial Nonstationarity. *Geogr. Anal.* **1996**, *28*, 281–298. [CrossRef]
41. McMillen, D.P. Geographically Weighted Regression: The Analysis of Spatially Varying Relationships. *Am. J. Agric. Econ.* **2004**, *86*, 554–556. [CrossRef]
42. Luo, J.; Du, P.; Samat, A.; Xia, J.; Che, M.; Xue, Z. Spatiotemporal Pattern of $PM_{2.5}$ Concentrations in Mainland China and Analysis of Its Influencing Factors using Geographically Weighted Regression. *Sci. Rep.* **2017**, *7*, 40607. [CrossRef] [PubMed]
43. Lin, G.; Fu, J.; Jiang, D.; Hu, W.; Dong, D.; Huang, Y.; Zhao, M. Spatio-Temporal Variation of $PM_{2.5}$ Concentrations and, Their Relationship with Geographic and Socioeconomic, Factors in China. *Int. J. Environ. Res. Public Health* **2013**, *11*, 173–186. [CrossRef]
44. Gautam, S.; Patra, A.M.; Kumar, P. Status and chemical characteristics of ambient $PM_{2.5}$ pollutions in China: A review. *Environ. Dev. Sustain.* **2019**, *21*, 1649–1674. [CrossRef]
45. Wang, G.; Cheng, S.; Li, J.; Lang, J.; Wen, W.; Yang, X.; Tian, L. Source apportionment and seasonal variation of $PM_{2.5}$ carbonaceous aerosol in the Beijing-Tianjin-Hebei Region of China. *Environ. Monit. Assess.* **2015**, *187*, 143. [CrossRef] [PubMed]
46. Zhang, L.; Liu, Y.; Hao, L. Contributions of open crop straw burning emissions to $PM_{2.5}$ concentrations in China. *Environ. Res. Lett.* **2016**, *11*, 014014. [CrossRef]
47. Cai, B.; Li, W.; Dhakal, S.; Wang, J. Source data supported high resolution carbon emissions inventory for urban areas of the Beijing-Tianjin-Hebei region: Spatial patterns, decomposition and policy implications. *J. Environ. Manag.* **2018**, *206*, 786–799. [CrossRef]
48. Xue, J.; Li, J.; Zhang, X. Characteristics of Elemental Compositions of Ambient $PM_{2.5}$ during Sandstorm in Spring in Xinjiang. *J. Environ. Health* **2010**, *29*, 759–762.
49. Lu, D.; Xu, J.; Yang, D.; Zhao, J. Spatio-temporal variation and influence factors of $PM_{2.5}$ concentrations in China from 1998 to 2014. *Atmos. Pollut. Res.* **2017**, *8*, 1151–1159. [CrossRef]
50. Wang, W.Q.; Zhu, X.P.; Zheng, C.X.; Aikebaier, Y.; Liu, B.; Wei, L.Y. Speciation Analysis of Cd in PM10 and $PM_{2.5}$ during Heating Period in Urumqi. *Spectrosc. Spectr. Anal.* **2012**, *32*, 235.
51. National Railway Administration of the People's Republic of China. Available online: http://www.nra.gov.cn/xxgkml/xxgk/ (accessed on 17 April 2020).
52. Civil Aviation Administration of China. Available online: http://www.caac.gov.cn/XXGK/XXGK/index_172.html (accessed on 17 April 2020).
53. Gao, W. The function of an acre of forest. *Ctry. Agric. Farmer* **1996**, 45.
54. Lim, S.; Lee, M.; Czimczik, C.I.; Joo, T.; Holden, S.; Mouteva, G.; Santos, G.M.; Xu, X.; Walker, J.; Kim, S.; et al. Source signatures from combined isotopic analyses of $PM_{2.5}$ carbonaceous and nitrogen aerosols at the peri-urban Taehwa Research Forest, South Korea in summer and fall. *Sci. Total Environ.* **2019**, *655*, 1505–1514. [CrossRef] [PubMed]
55. Editorial department. China Mobile Source Environmental Management Annual Report (2019). *Minist. Energy. Environ.* **2019**, *41*, 1.
56. Liu, J.; Wu, D.; Fan, S. Distribution of Regional Pollution and the Characteristics of Vertical Wind Field in the Pearl River Delta. *Environ. Sci.* **2015**, *36*, 3989–3998.